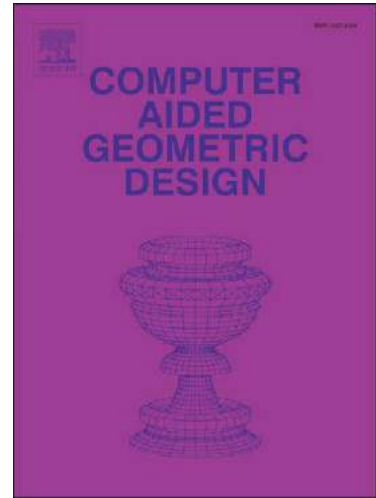# Accepted Manuscript

Geometric Accuracy Analysis for Discrete Surface Approximation

Junfei Dai, Wei Luo, Miao Jin, Wei Zeng, Ying He, Shing-Tung Yau, Xianfeng Gu

Geometric Accuracy Analysis for Discrete Surface Approximation

Junfei Dai [a], Wei Luo [a], Miao Jin [e], Wei Zeng [e,b], Ying He [c], Shing-Tung Yau [d], Xianfeng Gu [e,*]

[a]*Center of Mathematical Sciences, Zhejiang University, China.*
[b]*Institute of Computing Technology, Chinese Academy of Sciences, China.*
[c]*School of Computer Engineering, Nanyang Technological University, Singapore.*
[d]*Mathematics Department, Harvard University, MA, USA.*
[e]*Computer Science Department, Stony Brook University, NY, USA.*

Abstract

In geometric modeling and processing, computer graphics and computer vision, smooth surfaces are approximated by discrete triangular meshes reconstructed from sample points on the surfaces. A fundamental problem is to design rigorous algorithms to guarantee the geometric approximation accuracy by controlling the sampling density. This paper gives explicit formulae to the bounds of Hausdorff distance, normal distance and Riemannian metric distortion between the smooth surface and the discrete mesh in terms of principle curvature and the radii of geodesic circum-circle of the triangles. These formulae can be directly applied to design sampling density for data acquisitions and surface reconstructions. Furthermore, we prove that the meshes induced from the Delaunay triangulations of the dense samples on a smooth surface are convergent to the smooth surface under both Hausdorff distance and normal fields. The Riemannian metrics and the Laplace-Beltrami operators on the meshes are also convergent to those on the smooth surfaces. These theoretical results lay down the foundation for a broad class of reconstruction and approximation algorithms in geometric modeling and processing.

Practical algorithms for approximating surface Delaunay triangulations are introduced based on global conformal surface parameterizations and planar Delaunay triangulations. Thorough experiments are conducted to support the theoretical results.

Key words: Riemannian metric, Hausdorff distance, normal distance, Delaunay triangulation, principle curvature, discrete mesh

1. Introduction

In geometric modeling and processing, computer graphics and computer vision, smooth surfaces are often approximated by polygonal surfaces, which are reconstructed from a set of sample points. One of the fundamental problems is to measure the approximation accuracy in terms of position, normal fields and Riemannian metrics. It is highly desirable to design practical reconstruction algorithms with approximation errors fully controlled by the sampling density and triangulation method. This work accomplishes this goal by establishing the relation between the Hausdorff distance, normal field distance and the sampling density.

Different surface reconstruction algorithms have been discussed by many researchers. Hoppe et al. [1,2] represented the surface by the zero set of a signed distance function. Amenta et. al developed a series of algorithms based on Voronoi diagram in [3–5]. Bernardini and Bajaj used α shapes for manifold sampling and reconstruction [6,7]. Recently Ju et. al introduced the dual contour method for reconstruction [8]. Floater and Reimers reconstructed surfaces based on parameterizations [9]. Surface reconstruction has been applied to reverse engineering [10], geometric modelling [11], mesh optimization and simplification [12] and many other important applications.

It is a common belief that by increasing the sampling density, the reconstructed discrete mesh will approximate the smooth surface with any desired accuracy. This work aims at precisely formulating this common belief and rigorously prove it in an appropriate setting. This result will offer the theoretical guarantee for the general algorithms in geometric modelling and processing, where the measurements on smooth surface are calculated on its discrete approximations and the physical phenomena on original surface are simulated on the discrete counterpart.

* Corresponding author. Tel: 1(631)632-1828; Fax: 1(631)632-8334
  Email addresses: jfdai@cad.zju.edu.cn (Junfei Dai),
luowei@cms.zju.edu.cn (Wei Luo), mjin@cs.sunysb.edu (Miao Jin), zengwei@cs.sunysb.edu (Wei Zeng), yhe@ntu.edu.sg (Ying He), yau@math.harvard.edu (Shing-Tung Yau),
gu@cs.sunysb.edu (Xianfeng Gu).

1.1. *Geometric Accuracy*

There are different levels of accuracy when approximating a smooth surface by discrete meshes,

  (i) *Topological consistency*, it requires the surface and the mesh are homeomorphic to each other;

 (ii) *Positional consistency*, measured by Hausdorff distance between the surface and the mesh;

(iii) *Normal consistency*, it requires the normal fields on the surface and on the mesh are close to each other.

Many previous works address the theoretical guarantee of topological consistency. Leibon et al. proved in [13] that if the sampling density is high enough, the smooth surface and the triangle mesh induced by the Delaunay triangulation is homeomorphic. Amenta et al. proved a similar result in [5].

In terms of positional consistency, Amenta et al. invented a series of algorithms which reconstruct the meshes from sample points based on Voronoi diagrams. Assume the bound of the diameters of the face circum-circles is ε and the normal error is small enough, the Hausdorff distance between the mesh and the surface is bounded by the ε^2 in [5]. In [14], Elber introduced an algorithm to approximate freeform surfaces by discrete meshes with bounded Hausdorff distance.

Positional consistency does not guarantee the normal consistency. It is very easy to find a sequence of meshes, which converge to a smooth surface under the Hausdorff distance, but the normal field does not converge. In [15] and [16], Morvan and Thibert established theoretical results to estimate the normal error and area difference in terms of Hausdorff distance and angles on the triangulation.

The convergence of discrete Laplace-Beltrami operators over surfaces has been studied by Xu et al. in [17] and [18], where rigorous theoretical results are given. A statistical analysis of discrete laplace-Beltrami operators and their convergence properties is given by Hein, Audibert and Luxburg in [19].

In geometric modelling and processing, many algorithms require calculating the geodesics [20]. Many parametrization works require accurately approximating the Riemannian metrics [21]. Spectrum compression also needs good approximation of Laplace-Beltrami operators [22]. These important applications demand the theoretical guarantee for accurate approximation for Riemannian metric and differential operators. It has been shown in [23], Hausdorff convergence and normal field convergence guarantee the convergence of area, Riemannian metric tensor and Laplace-Beltrami operator.

Therefore, our work focuses on estimating both Hausdorff distance and normal field distance with the only assumption of the sampling density.

1.2. *Triangulations*

Triangulations play vital roles in surface reconstruction. There are different ways to measure the refinement of a triangulation,

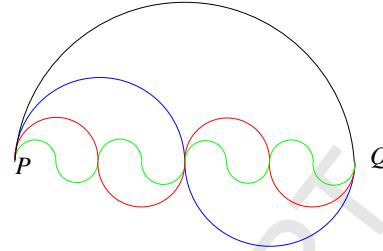 (i) The bound l of the longest lengths of the edges of triangles in the mesh.

Fig. 1. **Hausdorff convergence doesn't guarantee normal convergence and length convergence**. The black curve is a half circle with radius r, the blue curve is composed by two half circles with radii $\frac{r}{2}$; the red curve is composed by 4 half circles with radii $\frac{r}{4}$. A sequence of curves can be constructed, they converge to the diameter PQ under the Hausdorff distance. But the length of each of them equals to πr, which do not converge to the length of the diameter $2r$.

 (ii) The bound d of the diameters of the circum-circles of triangles in the mesh.

It is obvious that the diameter bounds the edge length, but the edge length does not bound the diameter(See Figure 2). In the following discussion, we will demonstrate that the Hausdorff distance is bounded by the square of the edge length, whereas the normal error is bounded by the diameter of the circum-circle.

In Figure 1, we demonstrate a one dimensional example, where a family of curves converge to a straight line segment under Hausdorff distance, but the lengths and normals do not converge.

In Figure 2, we demonstrate an example, where for the same sets of sample points, the bounds of edge lengths go to zero, but the bounds of the diameters of circum-circles remain constant. Therefore, neither the area nor the metric on the mesh converges to those on the smooth surface.

Given a dense set of sample points, it is highly desirable to find a triangulation such that the circum-circles are as small as possible. For sample points on the plane, Delaunay triangulation is a good candidate for such a triangulation. Leibon generalizes Delaunay triangulation to arbitrary Riemannian manifolds [13]. In the following discussion, we use Delaunay triangulation to refer Delaunay triangulation on surfaces. The Delaunay triangulation is determined solely by the sample points. In the following discussion, we will show that the meshes induced by the Delaunay triangulations are convergent both under Hausdorff distance and normal distance.

In practice, there is no prior knowledge of the smooth surface, only the dense sample points are available. The connectivity induced by the surface Delaunay triangulation can be best approximated using Voronoi diagram in $\mathbb{R}^3$ as described in [3,5]. We have not fully proven the consistency between the two triangulations.

1.3. *Factors Affecting Geometric Accuracy*

In order to achieve bounded Hausdorff error and normal error, the following factors play crucial rules, the sampling density should be carefully designed. The major factors determining the sampling density are as follows,
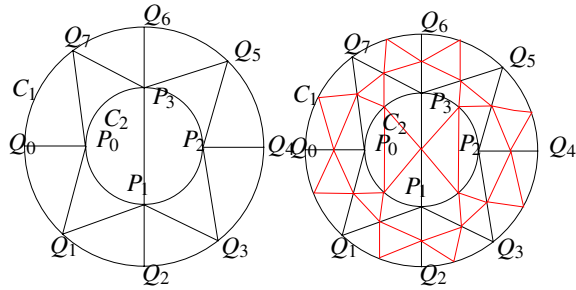
Fig. 2. **Hausdorff convergence vs. normal convergence**. In the left frame, the center is the north pole $(0,0,1)$ of the unit hemisphere. C_1 is the equator $x^2 + y^2 = 1$, C_2 is the intersection circle between the sphere with the plane $z = \frac{1}{2}$. All the arcs Q_iQ_j and P_iQ_j are geodesics, the arcs P_iP_j are arcs along C_2. The right frame shows one step subdivision: insert the middle points of all the arcs in the left frame, split each triangle to 4 smaller ones, such that if an edge connecting two points on C_2, the edge is the arc on C_2, otherwise the edge is a geodesic segment. Repeating this subdivision process to get a sequence of triangulations $\{T_n\}$, and a sequences meshes M_n induced by the triangulations. The longest edge length of T_n goes to zero, M_n converge to the hemi-sphere under Hausdorff distance. For any M_n there is one triangles f_0 adjacent to P_0 and contained in the curved triangle $P_1P_0P_3$. Because all three vertices of f_0 are on C_2, its circumscribe circle is C_2, the normal of f_0 is constant which differs from the normal at P_0 to the sphere. Therefore, $\{M_n\}$ doesn't converge to the sphere under normal distance.

– **Principle curvature** For regions with higher principle curvature, the samples should be denser.
– **Distance to medial axis** For regions closer to the medial axis, the samples should be denser to avoid topological ambiguity during the reconstruction process. It is also called local feature size.
– **Injectivity radius** Each point p on the surface M has a largest radius r, for which the geodesic disk $B(p,r)$ is an embedding disk. The injectivity radius of M is the infimum of the injectivity radii at each point. Each geodesic triangle on the surface should be contained in a geodesic disk with radius less than the injectivity radius.

These factors are not independent, but closely related. Suppose k is the bound of principle curvature on the surface, then the distance to the medial axis is no greater than $\frac{1}{k}$ as proved in [24].

1.4. *Comparisons to previous theoretical results*

Hildebrandt et.al's work [23] focuses on the equivalence of convergence of polyhedral meshes under different metrics, such as Hausdorff, normal, area and Laplace-Beltrami. Assuming the Hausdorff convergence and the homeomorphism between the surface and the mesh, all the error estimations are based on the homeomorphism.

Leibon et al's work [13] focuses on the existence of Delaunay triangulation for dense sample set. It only estimates the Riemannian metric error without considering Hausdorff error and normal error.

Amenta et al's work [5] only demonstrates the estimation of Hausdorff error under the two assumptions: first the sampling density is sufficiently high; second the normal field error is given and bounded.

Morvan and Thibert [15] [16] estimate the normal error and area difference in terms of Hausdorff distance and angles on the triangulation. In practice, in order to control both the Hausdorff distance and angles of triangulation, Chew's algorithm is applied to progressively add samples to reduce the Hausdorff distance and improve the triangulation.

Previous works either assume the normal error is bounded and estimate the Hausdorff distance or assume the Hausdorff distance is given and estimate the normal field error. In contrast, our work shows that solely the radii of geodesic circum-circles of faces on the triangulations are enough to guarantee the convergence of both Hausdorff distance and the normal fields. To the best of our knowledge, our work is the first one to bound both the Hausdorff error and the normal error (therefore the Riemannian metric distortion) only by the sampling density.

The main theorem of the work is that if the sampling density is ε, then the Hausdorff distance is no greater than $4k\varepsilon^2$, and the normal error is no greater than $9k\varepsilon$, where k is the upper bound of the principle curvature on the smooth surface to be approximated. The metric distortion is measured by the infinitesimal length ratio, which is bounded by $1 - 4k^2\varepsilon^2$ and $\frac{1+4k^2\varepsilon^2}{1-9k\varepsilon}$.

The paper is organized as the following, section 2 introduces the preliminary concepts and theorems proven in previous works; our new theoretical results are explained in details in section 3, which is the most technical part of the work, focusing on the proofs of three major theorems; practical algorithms for approximating surface Delaunay triangulation is introduced in section 4; experimental results are demonstrated in section 5; finally the paper is concluded in section 6, where the future works are briefly discussed.

2. Definitions and Preliminaries

In this section, we review the preliminary concepts necessary for our further theoretical arguments. We adopt the definitions from [13],[23], [3] and [5].

We assume that the surface S is closed without any boundary, at least C^2 smooth with bounded principle curvature, embedded in $\mathbb{R}^3$.

2.1. *Medial axis, ε-sampling and Delaunay triangulation*

The *medical axis* of a surface S embedded in $\mathbb{R}^3$ is the closure of the set of points with more than one nearest neighbor in S. The *local feature size* $f(p)$ at point $p \in S$ is the least distance of p to the medial axis.

A geodesic disk $B(p,r)$ centered at p with radius r is the point sets

$$B(p,r) = \{q \in S | d(p,q) \le r\},$$

d is the geodesic distance on the surface. The *injectivity radius* at a point $p \in S$ is the largest radius $\tau(p)$, for which the geodesic disk $B(p,\tau(p))$ is an embedding on S.

Suppose $\varepsilon : S \to \mathbb{R}$ is a positive function defined on the surface S, a point set $X \subset S$ is an ε-*sample*, if for any point $p \in S$, there is at least one sample inside the geodesic disk $B(p,\varepsilon(p))$.

The definition of Delaunay triangulations of X on S is the same as it is in $\mathbb{R}^2$. They are defined as having the empty circumscribing circle property: the circum-circle for each geodesic triangle contains no vertices of the triangulation in its interior. In order to guarantee the uniqueness and embedding of the circum-circles, X should be dense enough.

Leibon et al. proved in [13] that, suppose X is a generic ε-sample, ε satisfies the following conditions:

$$\varepsilon(p) \leq \min\{\frac{2\tau(p)}{5}, \frac{2\pi}{5k(p)}\}, \tag{1}$$

where $k(p)$ is the upper bound of the principle curvature, $k(p) = \max_{q \in B(p, \tau(p))} |k(q)|$, then the Delaunay triangulation of X exists and is unique.

2.2. Hausdorff Distance, Normal Distance and Shortest Distance Map

Let $M_1, M_2 \subset \mathbb{R}^3$ be non empty point sets, the *Hausdorff distance* between M_1 and M_2 is defined as

$$d_H(M_1, M_2) = \inf\{\varepsilon > 0 | M_1 \subset U_\varepsilon(M_2), M_2 \subset U_\varepsilon(M_1)\}, \tag{2}$$

where $U_\varepsilon(M) = \{x \in \mathbb{R}^3 | \exists y \in M : d(x, y) < \varepsilon\}$.

Suppose S and M are two surfaces embedded in $\mathbb{R}^3$, the shortest distance map $g : M \to S$ is defined to map $p \in M$ to its nearest point $g(p)$ on S. It is proved that the line connecting p to $g(p)$ is along the normal direction at $g(p)$ on S. It has been proven in [13], if the sampling density ε satisfies the Delaunay triangulation condition equation 1 and the following

$$\varepsilon(p) \leq \frac{f(p)}{4}, \tag{3}$$

where $f(p)$ is the local feature size at p, then the g is a homeomorphism between the mesh M and S induced by the Delaunay triangulation. Then we denote the inverse of g as $\Phi = g^{-1} : S \to M$ and call it the *inverse shortest distance map*, then

$$\Phi(p) = p + \phi(p)\mathbf{n}(p), p \in S \tag{4}$$

where $\mathbf{n}(p)$ is the normal vector at p on S, $\phi(p)$ measures the distance from p to $\Phi(p)$ on the mesh. The normal distance between S and M is defined as

$$d_n(S, M) = \max_{p \in S} |\mathbf{n}(p) - \mathbf{n} \circ \Phi(p)|.$$

Suppose $\gamma : t \to S$ is a curve on S, then $\Phi \circ \gamma : t \to M$ is a curve on M. It is proven in [23], the infinitesimal distortion of length satisfies

$$\min_i(1 - \phi k_i) \leq \frac{dl_M}{dl} \leq \max_i \frac{1 - \phi k_i}{<\mathbf{n}, \mathbf{n} \circ \Phi>}, \tag{5}$$

where $dl = \sqrt{<d\gamma, d\gamma>}$ is the length element on S, $dl_M = \sqrt{<d\gamma \circ \Phi, d\gamma \circ \Phi>}$ is the corresponding length element on M, k_i is the principle curvature.

3. Geometric Accuracy Analysis

In this section, we analyze the geometric accuracy of reconstructed meshes. Suppose X is an ε-sample on S, if ε satisfies

equation 1 then X induces a unique Delaunay triangulation T, where all edges are geodesics. Each face on T has a unique geodesic circumscribed circle, the bound of all the radii $r(X)$ is determined by the sampling density ε. Then by replacing geodesic triangles on T to Euclidean triangles, a piecewise linear complex $M(X)$ is produced, denoted as the *Delaunay mesh* induced by X. Our goal is to estimate the Hausdorff error, normal error and Riemannian metric error between S and M, in terms of the $r(X)$ and sampling density ε.

The following is the major steps of our proof,
  (i) We first estimate the Hausdorff distance between a geodesic triangle and the planar triangle through its vertices.
 (ii) Then we estimate the normal deviation between the normal at an arbitrary point in a geodesic triangle and the normal of the planar triangle.
(iii) Finally we discuss the Hausdorff distance and normal distance between S and M, then we estimate the metric distortion.

3.1. Hausdorff Distance Between a geodesic triangle and a planar triangle

Lemma 1. *Let $R(t)$ be an arc length parameterized smooth space curve with curvature bound $\kappa > 0$, $0 \leq a, b, t, t' \leq \pi/\kappa$, $m = \frac{R(b) - R(a)}{|R(b) - R(a)|}$ then the following estimates hold*

$$t \geq |R(t) - R(0)| \geq 2\sin(\kappa t/2)/\kappa \tag{6}$$

$$|R'(t) \times m| \leq \frac{1}{4}\kappa(b - a), \ t \in [a, b], \kappa(b - a) < \sqrt{6} \tag{7}$$

$$|R'(t') - R'(t)| \leq |2\sin(\kappa(t - t'))| \tag{8}$$

$$\angle R(a)R(t)R(b) \geq \pi/2 \tag{9}$$

$$\text{dist}(R(t), R(a)R(b)) \leq \frac{\kappa(b - a)\min(t - a, b - t)}{4}, \tag{10}$$

$$0 < a < t < b < \sqrt{6}/\kappa$$

$$0 < (R(t) - R(a), m) < |R(b) - R(a)|, \quad t \in (a, b) \tag{11}$$

where $\text{dist}(\cdot, \cdot)$ denote the distance from a point to a line, and $(\cdot, \cdot)$ denotes the inner product of two vectors.

Proof. Consider function $f(t) = (R'(t), R'(0))$, then since $R'(t) \perp R''(t)$,

$$f'(t) = (R''(t), R'(0)) = (R''(t), R'(0) - (R'(0), R'(t))R'(t))$$
$$\geq -\kappa|R'(t) \times R'(0)| = -\kappa\sqrt{1 - f^2(t)}$$

$f(t)$ satisfies $f'(t) \geq -\kappa\sqrt{1 - f^2(t)}$, $f(0) = 1$, then

$$\frac{\partial}{\partial t}(\arccos f(t)) \leq \kappa$$
$$f(t) \geq \cos(\kappa t), \quad t \in [0, \pi/\kappa]$$

Now the estimates follows by integration:

4

$$|R(t) - R(0)|^2 = \int_0^t \int_0^t (R'(t_1), R'(t_2)) \, dt_1 dt_2$$
$$\geq \int_0^t \int_0^t \cos(\kappa(t_2 - t_1)) \, dt_1 dt_2$$
$$= 4\kappa^{-2} \sin^2(\kappa t/2) \quad \Rightarrow (6)$$

$$|R(b) - R(a)|(R'(t), m) \geq \int_a^b \cos\kappa(s - t) \, ds$$
$$= \frac{1}{\kappa}(\sin\kappa(b - t) + \sin\kappa(t - a)) \quad (12)$$
$$\geq (b - a) - \frac{\kappa^2(b - a)^3}{6}$$

$$|R'(t) \times m| = \sqrt{1 - (R'(t), m)^2}$$
$$\leq \sqrt{1 - (1 - \kappa^2(b - a)^2/6)^2}, \text{ if } \kappa(b - a) < \sqrt{6}$$
$$\leq \frac{\sqrt{2}}{6}\kappa(b - a) \quad \Rightarrow (7)$$

Equation (12) implies $(R'(t), R(b) - R(a)) > 0$ when $b - a < \pi/\kappa$, hence $(R(t), R(b) - R(a))$ is an increasing function of t, hence (11) is proved.

$$(R(b) - R(t), R(t) - R(a)) \geq \int_a^t \int_t^b \cos\kappa(u - v) \, du dv$$

the right hand side equals to

$$\cos\kappa(b - t) + \cos\kappa(t - a) - 1 - \cos(b - a) \geq 0$$
$$\text{if } \kappa(b - a) < \pi \quad \Rightarrow (9).$$

$$(R'(t), R'(t')) \geq \cos\kappa(t' - t), \quad |R(t)| = |R'(t')| = 1 \quad \Rightarrow (8)$$

Assume $t - a < b - t$, then (7) implies that

$$\text{dist}(R(t), R(a)R(b)) = |(R(t) - R(a)) \times m)| \leq \kappa(b - a)(t - a)/4$$

which $\Rightarrow$ Eqn(10). $\square$

Notation: We use $\widetilde{}$ to denote an geometric object on a surface in geodesic sense, such as $\widetilde{AB}$, $\widetilde{\Delta ABC}$ to denote a geodesic or a geodesic triangle.

Lemma 2. *P, Q are two points in a geodesic convex region of a smooth surface with principal curvature bounded by* κ*, then the normal at P, Q differs by at most* $\kappa|\widetilde{PQ}|$*.*

Proof. Bound of principal curvature implies $|\nabla n| \leq \kappa$, where ∇ is the covariant derivative and n is the normal. Hence the estimate. $\square$

The following theorem estimate the distance of points inside a geodesic triangle to the plane through the vertices, independent of the shape of the triangle.

Theorem 1. *Let* $\widetilde{\Delta ABC}$ *be a geodesic triangle on a smooth surface embedded in* $\mathbb{R}^3$ *where the principal curvature is bounded by* κ *and the maximal length d of edges of* $\widetilde{\Delta ABC}$ *is bounded by* $1/\kappa$*. P is any point inside the triangle,* P_{ABC} *is the plane through A, B, C, then the* $\text{dist}(P, P_{ABC}) \leq \kappa d^2/4$*.*

Proof. Assume $\widetilde{AP}$ intersects $\widetilde{BC}$ at Q, P' is the projection of P onto AQ, Q projects onto BC at H, H' is on AH such that $P'H'$ is parallel to QH. By (10),

$$\text{dist}(Q, P_{ABC}) \leq \text{dist}(Q, BC) = |QH| \leq \kappa d^2/8.$$
$$|PP'| \leq \kappa d^2/8$$

(11) implies that P' is inside AQ and $|P'H'| \leq |QH|$,

$$\text{dist}(P, P_{ABC}) \leq |PP'| + |P'H'| \leq \kappa d^2/4$$

$\square$

From the proof we see that when P go through $\widetilde{\Delta ABC}$, H' go through ΔABC. Then it is easy to see that the nearest distance of any point on ΔABC is also bounded by $\kappa d^2/4$. Thus we have the following corollary.

Corollary 3. *With the same assumption of* $\widetilde{ABC}$ *and* κ, d*. The shortest distance of and point in ABC to* $\widetilde{ABC}$ *is bounded by* $\kappa d^2/4$*.*

3.2. *Normal Error Estimation between a geodesic triangle and a planar triangle*

Lemma 4. *Let* $\widetilde{ABC}$ *be a geodesic triangle with maximal length of edge d, the principal curvature is bounded by* κ*,* $d < 2/\kappa$*,* $\angle BAC = \alpha$*, then the normal* n_A *to the surface at A and the normal n to* P_{ABC} *satisfies*

$$|n_A \times n| \leq \max\left(\frac{\kappa d}{4\sin(\alpha/2)}, \frac{\kappa d}{4\cos(\alpha/2)}\right) \quad (13)$$

Proof. Denote by T_1 the tangent vector at A to $\widetilde{AB}$, T_2 tangent to $\widetilde{AC}$, V_1 the unit vector along AB, V_2 along AC. Then by (7)

$$|T_1 \times V_1| \leq \kappa d/4, |T_2 \times V_2| \leq \kappa d/4$$

So

$$|(n_A, V_1)| = |(n_A, V_1 - (V_1, T_1)T_1)|$$
$$\leq |V_1 - (V_1, T_1)T_1| = |T_1 \times V_1| \leq \kappa d/4$$
$$|(n_A, V_2)| \leq \kappa d/4$$

The projection of n_A onto P_{ABC} falls into the parallelogram with both width $\kappa d/2$ and inner angle $\alpha, \pi - \alpha$, centered at A. Now (13) follows by simple trigonometry. $\square$

Lemma 5. *Let* $l(t)$ *be a geodesic circle radius r, parameterized by arc length. Suppose the principal curvature is bounded by* κ *in the disk and* $r \leq 1/(4\kappa)$*.* $N(t)$ *is the tangent vector at* $l(t)$ *normal to* $l'(t)$*. Then for* $t < r$*,*

$$(l(t) - l(0), N(0)) \geq \frac{t^2}{5r} \quad (14)$$

Proof. Let $n(t)$ be the normal to the surface at $l(t)$. The curvature condition implies $|(l''(t), n(t))| \leq \kappa$. Hessian comparison theorem [25] implies

5

$$(l''(t), N(t)) \geq \kappa \cot(\kappa r) \geq \frac{19}{20r}, \quad \text{if } \kappa r < 1/4$$

$$|l''(t)| \leq \kappa\sqrt{\coth \kappa r^2 + 1} \leq \frac{11}{10r}, \quad \text{if } \kappa r < 1/4 \qquad (15)$$

Lemma 3.1 implies $|n(t) - n(0)| \leq \kappa t$. (15) implies $|l'(t) - l'(0)| \leq 11t/10r$, then for $t \leq r$

$$\begin{aligned}
(l''(t), N(0)) &= (l''(t), N(t)) + (l''(t), N(0) - N(t)) \\
&= (l''(t), N(t)) + (l''(t), n(0) \times l'(0) - n(t) \times l'(t)) \\
&\geq (l''(t), N(t)) - |l''(t)|(|n(0) - n(t)| + |l'(0) - l'(t)|) \\
&\geq \frac{1}{r}(\frac{19}{20} - \frac{11\kappa t}{10} - \frac{121t}{100r})
\end{aligned} \qquad (16)$$

Use $l'(0) \perp N(0)$, integrate (16) to get

$$(l(t) - l(0), N(0)) \geq \frac{9t^2}{40r}$$

$\square$

Theorem 2. *D is a geodesic disk of radius r of a smooth surface embedded in $\mathbb{R}^3$ with principal curvature bounded by κ, $r < 1/(4\kappa)$. A, B, C are three distinct points on the boundary of D, P_{ABC} is the plane through A, B, C, Φ is the inverse shortest distance map from D onto P_{ABC}. For any point $p \in D$, $v \in T_p$ is a tangent vector, we have*

$$|n_p - n_{ABC}| \leq 4.5\kappa r \qquad (17)$$
$$|v| \geq |\Phi_*(v)| \geq |v|(1 - 4.5\kappa r) \qquad (18)$$
$$\text{dist}(p, P_{ABC}) \leq 9\kappa r^2 \qquad (19)$$

Proof. Consider the intersection angle between the radial geodesic connecting center O of D and the vertices A, B, C.

If two such intersection angle is less than $9/10$, say $\angle \widetilde{AOB}, \angle \widetilde{BOC}$, then comparison theorem shows that the arc between A, B or between B, C along boundary of D is less than

$$\frac{9}{10} \cdot \frac{e^{\kappa r} - e^{-\kappa r}}{2\kappa} \leq r \qquad (20)$$

Let d_1, d_2 be the length of line segment AB, BC respectively, then (11) implies $\angle ABC > \pi/2$ while Lemma 3.2 implies

$$\angle ABC \leq \pi - \arcsin(d_1/5r) - \arcsin(d_2/5r)$$

Then apply Lemma 4 to get

$$|n_B - n_{ABC}| \leq \frac{\kappa(d_1 + d_2)}{4\cos(\angle ABC)/2} \leq \frac{\kappa(d_1 + d_2)}{2d_1/5r + 2d_2/5r} = 2.5\kappa r$$

If only one such intersection angle is less than $9/10$, say $\angle \widetilde{AOB}$, without lost of generality, assume $\angle BAC \geq \angle ABC$. For the triangle AOC, by (6) and (7)

$$\angle AOC \geq 9/10 - 2\arcsin(\kappa r/4) \geq 0.77$$
$$r > |OA|, |OC| > .99r$$
$$|AC| \geq 2 * .99 \sin(0.77/2)r > 0.74r \qquad (21)$$
$$\angle CAO \leq \arccos((.99^2 + .74^2 - 1)/(2 * .99 * .74)) < 1.21$$
$$\angle BAO \leq \pi/2 + 2\arcsin(\kappa r/4) \leq 1.70$$
$$4\cos(\angle(CAB)/2) \geq 4\cos(1.455) \geq 0.46 \qquad (22)$$

On the other hand for ΔABC, $|AC|, |BC| \geq 0.74r$ by (21), $|AB| \leq r$ by (20), so

$$\angle BAC \geq \arccos(.5/.74) \geq .8$$
$$4\sin(\angle BAC/2) \geq 1.4 \qquad (23)$$

Now apply Lemma 4 with estimate (22) and (23) to give an estimate of the difference of the normal at A and to the plane ABC, then use Lemma 3.1 to get (17).

Given (17) proved, (18) easily follows as

$$|v - \Phi_*(v)| = |(v, n_{ABC})| = |(v, n_{ABC} - n_A)| \leq 4.5\kappa r|v|$$

and for (19), let $l(t)$ be the geodesic connecting A and p

$$\text{dist}(p, P_{ABC}) = |\int_l (l'(t), n_{ABC})dt| \leq \widetilde{\text{dist}}(p, A) * 4.5\kappa r \leq 9\kappa r^2$$

$\square$

3.3. *Geometric Accuracy for Delaunay Meshes*

Combining the theoretical results in section 2 and the estimations on a single geodesic triangle theorem 3.1 and theorem 3.2, we can easily get the following theorem.

Theorem 3. *Suppose S is a closed C^2 smooth surface embedded in $\mathbb{R}^3$. The principle curvature upper bound is k, the injective radius lower bound is τ, the lower bound of local feature size is f. Suppose X is an ε-sample set on S, such that constant ε satisfies the following conditions,*

$$\varepsilon \leq \min\{\frac{2\tau}{5}, \frac{2\pi}{5k}, \frac{f}{4}, \frac{1}{8k}\},$$

then X induces a unique Delaunay triangulation T, (X, T) induces a piecewise linear complex M,

(i) M is homeomorphic to S, the nearest distance map $g: M \to S$ is a homeomorphism.

(ii) The Hausdorff distance

$$d_H(M, S) \leq 4k\varepsilon^2 \qquad (24)$$

(iii) The normal distance

$$d_n(M, S) \leq 9k\varepsilon \qquad (25)$$

(iv) The infinitesimal length ratio

$$1 - 4k^2\varepsilon^2 \leq \frac{dl_M}{dl} \leq \frac{1 + 4k^2\varepsilon^2}{1 - 9k\varepsilon}. \qquad (26)$$

Proof. Because X is an ε-sample, ε satisfies the Delaunay triangulation condition in Equation (1), therefore the unique Delaunay triangulation T exists according to [13]. ε is less than a quarter of the local feature size (3), then the shortest distance map is a homeomorphism.

Suppose C is a circumscribe circle of a triangle in T, then there is no interior point belonging to X. If the radius of C is greater than 2ε, then C contains at least disks with radii ε, therefore, it contains at least one point of X as its interior. Thus the radius of C is no greater than 2ε.

From corollary 3.1, the Hausdorff distance is no greater than $4k\varepsilon^2$. From the proof of theorem 2, the normal distance at some sample point is less than $5k\varepsilon$, also from (24) and previous

paragraph, any point on X is within 4ϵ distance to such a sample point, thus together with Lemma 2, the normal distance at any point is no greater than $9k\epsilon$.

In the inverse shortest distance map Eqn. (4), ϕ is less or equal to the Hausdorff distance. From formula (5) we can derive the (26). □

Although the sampling density ϵ is a constant here, it can be generalized to be a function on the surface, such that

$$\epsilon(p) \leq \min\{\frac{2\tau(p)}{5}, \frac{2\pi}{5k(p)}, \frac{f(p)}{4}, \frac{1}{8k(p)}\},$$

then we can estimate the Hausdorff distance, normal distance and metric distortion at point p using the formula similar to (24),(25),(26) with ϵ replaced by $\epsilon(p)$.

4. Approximation of Surface Delaunay Triangulation

Theoretical surface Delaunay triangulation is impractical, because the geodesic circles are difficult to compute. In this work, we propose to use global conformal parameterization to map the surface to the canonical domains, and compute the Delaunay triangulation on the conformal parametric domains to approximate the surface Delaunay triangulation. Delaunay triangulations maximize the minimal angle, conformal parameterization preserves angles, therefore, Delaunay triangulations on conformal parametric domains approximate the surface Delaunay triangulations faithfully.

4.1. *Global Conformal Surface Parameterizations*

Suppose S_1 and S_2 are two surfaces with Riemannian metrics $\mathbf{g}_1$ and $\mathbf{g}_2$, suppose $f : S_1 \rightarrow S_2$ is a map, then if the original metric $\mathbf{g}_1$ and the pull back metric $f^*\mathbf{g}_2$ differ by a scalar

$$e^{2u}\mathbf{g}_1 = f^*\mathbf{g}_2, u : S_1 \rightarrow \mathbb{R},$$

then f is a *conformal* map. A conformal map preserves angles.

Suppose S_1 and S_2 are embedded in the Euclidean space, the *harmonic energy* of f is defined as

$$E(f) = \int_{S_1} |\nabla f|^2 dA.$$

For genus zero closed surfaces, harmonic maps are conformal and all of them can be conformally mapped to the unit sphere $\mathbb{S}^2$. Suppose S is a genus zero closed surface, we can get a conformal map from S to $\mathbb{S}^2$ by diffusing its Gauss map using the following heat flow method

$$\frac{df}{dt} = -\Delta f,$$

with a constraint $\int_S f dA = 0$, where Δ is the Laplace-Beltrami operator on S. The heat flow will converge, the final map is a conformal map. Figure 6 demonstrates a conformal spherical parameterization for a genus zero closed surface. Once the surface is mapped to a unit sphere, we can use steoreo-graphic projection to conformally map the sphere onto the plane. For details, we refer readers to the work of [26]. This method can

be generalized to compute conformal structures of general surfaces [27]. The rigorous theoretical proof for the convergence of the algorithm can be found in [28]. Figure 6 illustrates the global conformal parameterization for a genus zero closed surface.

For surfaces with non-zero genus, the *Ricci flow* is a powerful method to compute the conformal parameterization. Suppose $\mathbf{g} = (g_{ij})$ is the initial Riemannian metric on a surface S, then the *Ricci flow* is defined as

$$\frac{dg_{ij}(t)}{dt} = -Kg_{ij}(t),$$

where K is the Gaussian curvature. Then it is proven that Ricci flow will converge, the final metric $\mathbf{g}(\infty)$ is conformal to the original metric and induces a constant Gaussian curvature. Therefore, the surfaces can be conformally parameterized by the Euclidean plane (genus one case) or the hyperbolic disk (high genus case). Figure 4 demonstrates a genus one surface conformally parameterized using Ricci flow method; Figure 7 shows a genus two surface conformally mapped to the hyperbolic disk using Ricci flow method.

The discrete algorithms for heat flow can be found in [29], the discrete Ricci flow method can be found in [30]. Figure 4 and 7 demonstrate global conformal parameterizations for high genus surfaces.

4.2. *Approximation of Surface Delaunay Triangulation*

After conformal parameterization of the surface, we generate random samples on the parameter domain and construct a planar Delaunay triangulation which induces an approximation of the surface Delaunay triangulation. This method was proposed in [31] for topological disk case. In current work, we generalize the algorithm for arbitrary surfaces.

We use a piecewise polygonal mesh to represent the surface, suppose the surface has n faces $\{f_1, f_2, \cdots, f_n\}$, then we use the following sampling and Delaunay re-meshing algorithm:

(i) Compute a global conformal surface parameterization of the input mesh.

(ii) Compute $g(i) = \sum_{k=1}^{i} s_k$, where s_k is the area of face f_i on the original surface.

(iii) Generate a random number $r \in [0, 1]$ with the uniform distribution. Find the unique i, such that $r \in [g(i-1)/g(n), g(i)/g(n)]$, then the sample point should be on face f_i.

(iv) Suppose the three vertices of f_i are v_1, v_2, v_3, generate another two independent random numbers α, β, such that both of them are uniform distributed. Then the barycentric coordinates of the sample on f_i is $(\alpha, (1-\alpha)\beta, (1-\alpha)(1-\beta))$.

(v) The position of the sample in $\mathbb{R}^2$ is the linear combination of the positions of v_is, the coefficients are the barycentric coordinates. The parameter of the sample is the linear combination of the parameters of the v_i's using the barycentric coordinates.

(vi) Repeat step 2 through 4 to generate random samples, compute the Delaunay triangulation on the parametric

7

Shape	# vertices	# faces	D	κ	d	$1/4\kappa d^2$
sphere	1002	2000	0.010025	1.758418	0.314097	0.014678
torus	240	480	0.049931	4.525904	0.616819	0.065040
knot	2000	4000	0.032552	9.280646	0.391005	0.053959

Table 1
Comparison between the theoretical prediction of the Hausdorff distance and the real measured distance. D is the measured Hausdorff distance; $\frac{1}{4}\kappa d^2$ is the theoretical estimations, where κ is the maximal principal curvature, d is the maximal length of edges.
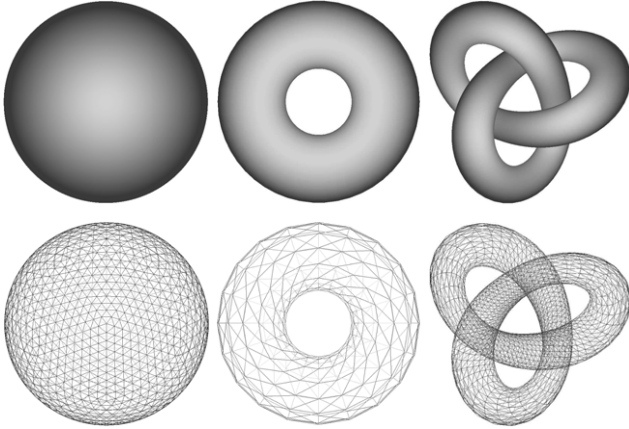

Fig. 3. Smooth surfaces are approximated by Delaunay meshes. The Hausdorff distances really measured are consistent with the theoretical formulae.

domain, which induces a polygonal mesh in $\mathbb{R}^3$.

The Delaunay re-meshing results are shown in Figures 4,5, 6 and 7.

5. Experimental Results

In order to verify our theorems, we tessellate several smooth surfaces with different resolutions, for each mesh, we measure the upper bound of the diameters of the faces, the upper bound of the radii of the circum-circles of the faces. We also measure the Hausdorff distance and the normal distance between the mesh and the smooth surface. The experimental results shows the Hausdorff distance is quadratically convergent with respect to the diameter of the face, the normal distance convergent linearly with respect to the circum-circle radius. These experiments results are consistent with our theorems.

Table 1 and Figure 3 illustrate the comparison between numerical results and the theoretical estimation of Hausdorff distance for some simple surfaces. The surfaces have explicit representations, therefore the computation of curvature bound is straight forward. Then we tessellate the surface on the parameter domain. We estimate the diameter of triangles using the Euclidean distances between the vertices. The Hausdorff distance is calculated by minimizing the following functional, suppose $p \in M$, S is $S(u,v)$ then $f(u,v) = < S(u,v) - p, S(u,v) - p >$. For any point p on M, first we find the closest vertex p_0 on M, p_0 is also on S with parameter (u_0, v_0). Then we use (u_0, v_0) as the initial point, then use Newton's method to find the global
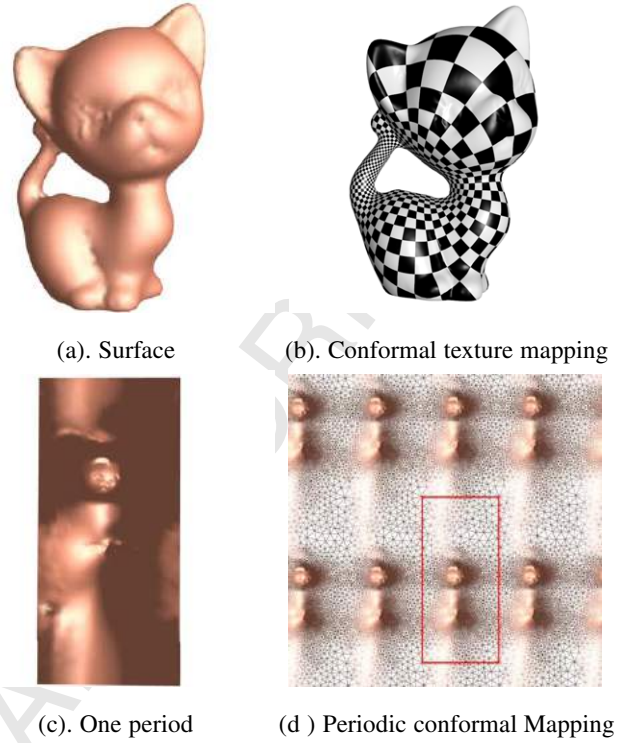

(a). Surface   (b). Conformal texture mapping

(c). One period (d) Periodic conformal Mapping

Fig. 4. Global conformal surface parameterization for a genus one closed surface, the parameterization is periodic.

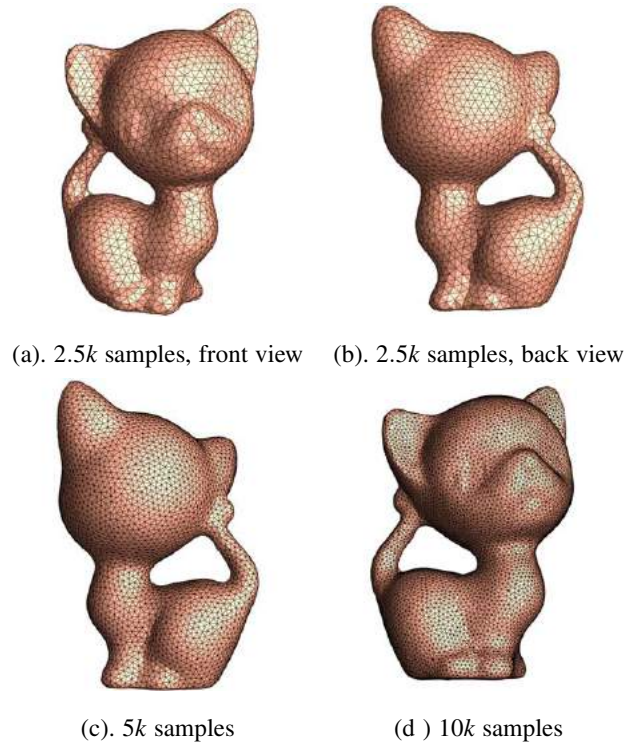(a). 2.5k samples, front view (b). 2.5k samples, back view

(c). 5k samples   (d) 10k samples

Fig. 5. Approximated surface Delaunay triangulation by global conformal parameterization. The sample points are 2.5k, 5k and 10k.

(a). Original surface.　　　(b). Spherical conformal mapping.

(c). Delaunay triangulation,
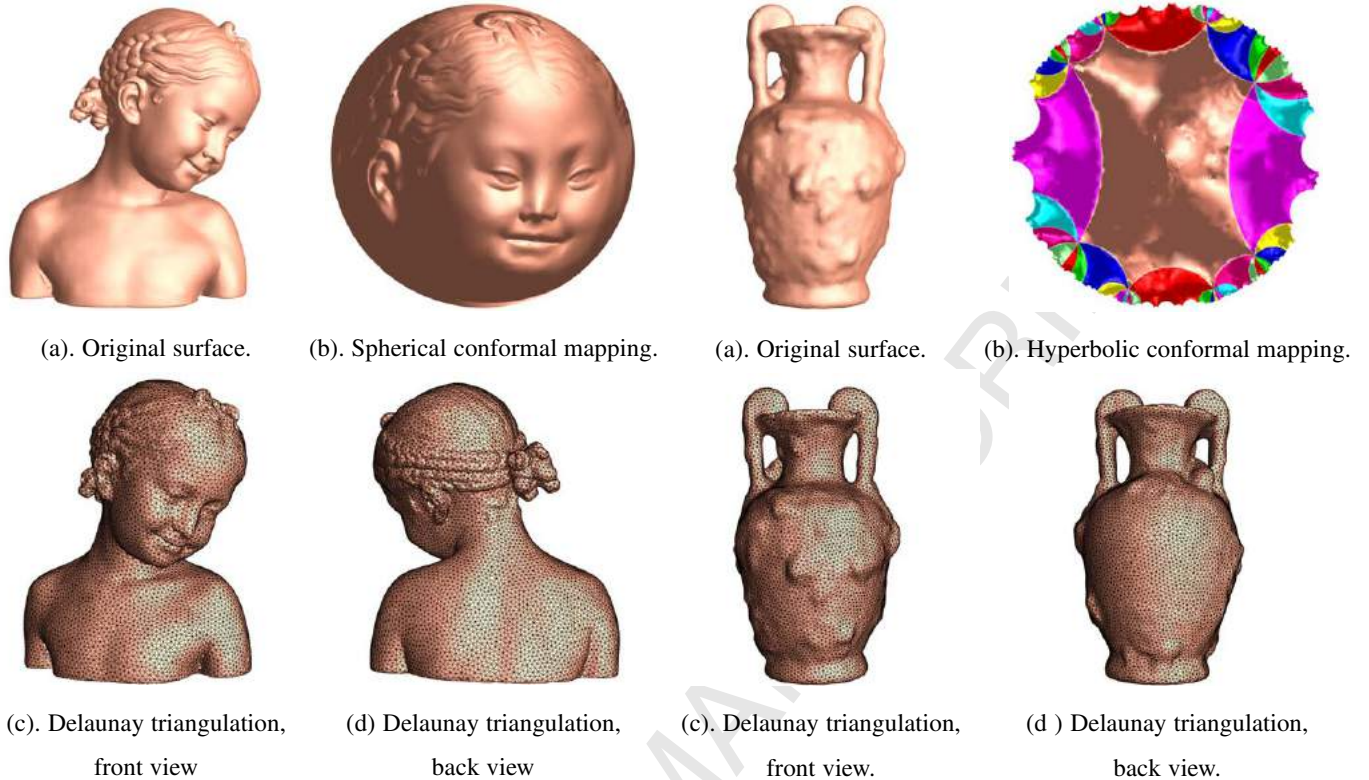
front view

(d) Delaunay triangulation,

back view

Fig. 6. Approximated surface Delaunay triangulation by global conformal parameterization for a genus zero closed surface. The sample points are 10*k*.

(a). Original surface.　　　(b). Hyperbolic conformal mapping.

(c). Delaunay triangulation,

front view.

(d) Delaunay triangulation,

back view.

Fig. 7. Approximated surface Delaunay triangulation by global conformal parameterization for a genus two closed surface. The sample points are 10*k*.

minimum of $f(u, v)$. We densely sample M, and find the maximum distance between the sample points to S. we subdivide the triangulation on the parameter domain to get a sequence of meshes. The diameters of faces converge to zero, the radii of circum-circles converge to zero, the largest angle are bounded. From the table, it is clear that the numerical results are always no greater than the theoretical upper bound, and the real values are close to their theoretical predictions.

We further verify our theoretical results by several complicated surfaces as illustrated in Figure 8. All the models are scaled into a unit cube. In order to accurately compute the principal curvature, Hausdorff distance and normal, we convert these shapes into manifold splines [32][33][34]. We construct the manifold triangular *B*-splines for the two-hole torus (of genus 2, the second row in figure 8) and sculpture (of genus 3, the third row in figure 8), and manifold T-spline for the kitten model (of genus 1, the first row in figure 8). We compute the curvature bound using the spline function. We then tessellate the spline surfaces by triangulating the parameter domain to induce a polygonal mesh. Next we subdivide the planar triangulation to get the refined meshes. For each mesh, we compute the diameter of the faces d and the Hausdorff distance d_H between the spline surface and the mesh. We plot the points of (d, d_H), which form a quadratic curve (see Figure 9(a)). Also, we compute the bound of the radii of the circum-circles of faces on each mesh r, and the normal distance d_N. We plot the pairs (r, d_N), which form a linear curve when r is sufficiently small

(see Figure 9(b)). The experimental results are consistent with our theoretical predictions.

6. Conclusion and Future Work

This work gives explicit formulae of approximation error bounds for both Hausdorff distance and normal distance in terms of sampling density. For a set of sample points on a surface with sufficient density, it induces a unique Delaunay triangulation, and a discrete mesh. With the increase of sampling density, the Delaunay meshes converge to the original surface under both Hausdorff distance and normal distance, therefore, the area, the Riemannian metrics and the Laplace-Beltrami operators are also convergent.

The theoretical results can be directly generalized along two directions: general triangulations and off surfaces samples.

(i) **General Triangulations** From our theoretical deduction, the Hausdorff distance is bounded by the quadratic function of the diameter of triangles on the discrete mesh, the normal distance is bounded by the radius of the circumcircle of the triangle on the mesh. The results proved in this paper works for Delaunay triangulation, same estimates(but may with different constants) work for triangulations where the largest angle of any face is bounded. For example it will work for a triangulation with only acute triangles. The proof is a direct application of Lemma 4.

9

Fig. 8. Manifold splines are used to verify the theoretical results. These spline surfaces are of C^2 continuous, thus, the principal curvatures, normals, Hausdorff distance, etc, can be obtained analytically.

(ii) **Samples off the surface** In this paper, the sample points are assumed to be on the surface. When sample points are off the surface in practice, we expect the same results to be valid if the normal distance of the sample points is up to a constant locally bounded by the square of least distance between sample points, thus the geometric accuracy results are expectable.

A practical algorithm is introduced to approximate surface Delaunay triangulations using planar Delaunay triangulations on conformal parametric domains. The method produces good approximation results and is practical for real applications.

In the future, we will apply these error estimation formulae to prove the convergence of other advanced algorithms in geometric modeling and processing, such as the conformal parameterizations, Poisson editing etc. We will prove the convergence of current surface Delaunay triangulation algorithm.

Acknowledgements
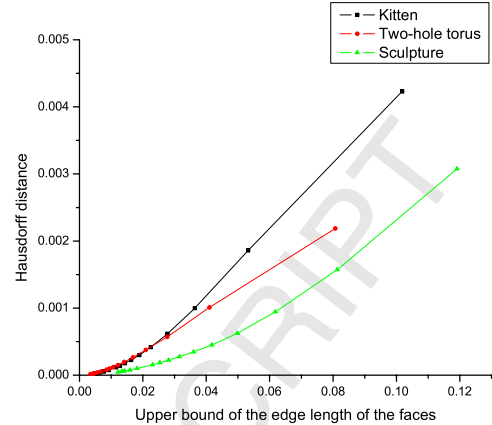
(a) Hausdorff distance converges quadratically to zero.
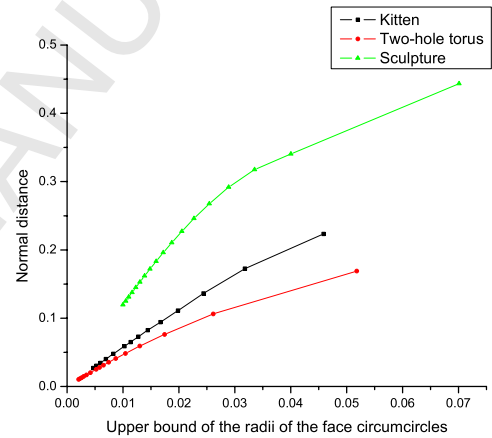
(b) Normal distance converges linearly to zero.

Fig. 9. Hausdorff distance and normal distance converge to zero.

References

[1] Hoppe, H., DeRose, T., Duchamp, T., McDonald, J.A., Stuetzle, W.: Surface reconstruction from unorganized points. In: SIGGRAPH. (1992) 71–78

[2] Eck, M., Hoppe, H.: Automatic reconstruction of b-spline surfaces of arbitrary topological type. In: SIGGRAPH. (1996) 325–334

[3] Amenta, N., Bern, M.W., Kamvysselis, M.: A new voronoi-based surface reconstruction algorithm. In: SIGGRAPH. (1998) 415–421

[4] Amenta, N., Bern, M.W.: Surface reconstruction by voronoi filtering. Discrete & Computational Geometry **22** (1999) 481–504

[5] Amenta, N., Choi, S., Dey, T.K., Leekha, N.: A simple algorithm for homeomorphic surface reconstruction. Int. J. Comput. Geometry Appl. **12** (2002) 125–141

[6] Bajaj, C.L., Bernardini, F., Xu, G.: Automatic reconstruction of surfaces and scalar fields from 3d scans. In: SIGGRAPH. (1995) 109–118

[7] Bernardini, F., Bajaj, C.L.: Sampling and reconstructing manifolds using alpha-shapes. In: CCCG. (1997)

[8] Ju, T., Losasso, F., Schaefer, S., Warren, J.D.: Dual contouring of hermite data. In: SIGGRAPH. (2002) 339–346

[9] Floater, M.S., Reimers, M.: Meshless parameterization and surface

reconstruction. Computer Aided Geometric Design **18** (2001) 77–92

[10] Benkö, P., Martin, R.R., Várady, T.: Algorithms for reverse engineering boundary representation models. Computer-Aided Design **33** (2001) 839–851

[11] He, Y., Qin, H.: Surface reconstruction with triangular b-splines. In: GMP. (2004) 279–290

[12] Hoppe, H.: Progressive meshes. In: SIGGRAPH. (1996) 99–108

[13] Leibon, G., Letscher, D.: Delaunay triangulations and voronoi diagrams for riemannian manifolds. In: Symposium on Computational Geometry. (2000) 341–349

[14] Elber, G.: Error bounded piecewise linear approximation of freeform surfaces. Computer Aided Design **28** (1996) 51–57

[15] Morvan, J., Thibert, B.: On the approximation of a smooth surface with a triangulated mesh. Computational Geometry Theory and Application **23** (2002) 337–352

[16] Morvan, J., Thibert, B.: Approximation of the normal vector field and the area of a smooth surface. Discrete and Computational Geometr **32** (2004) 383–400

[17] Xu, G.: Convergence of discrete laplace-beltrami operators over surfaces. Computers and Mathematics with Applications **48** (2004) 347–360

[18] Liu, D., Xu, G.: A discrete scheme of laplace-beltrami operator and its convergence over quadrilateral meshes. In Chen, F., Deng, J., Xu, C., eds.: Progress of Geometric Design and Computing in 2005, Press of University of Science and Technology of China (2005)

[19] Matthias Hein, Jean-Yves Audibert, U.v.L.: Graph laplacians and their convergence on random neighborhood graphs. arxiv.org/abs/math.ST/0608522 (2006)

[20] Surazhsky, V., Surazhsky, T., Kirsanov, D., Gortler, S.J., Hoppe, H.: Fast exact and approximate geodesics on meshes. ACM Trans. Graph. **24** (2005) 553–560

[21] Floater, M.S., Hormann, K.: Surface parameterization: a tutorial and survey. In Dodgson, N.A., Floater, M.S., Sabin, M.A., eds.: Advances in multiresolution for geometric modelling. Springer Verlag (2005) 157–186

[22] Ben-Chen, M., Gotsman, C.: On the optimality of spectral compression of mesh data. ACM Trans. Graph. **24** (2005) 60–80

[23] Hildebrandt, K., Polthier, K., Wardetzky, M.: On the convergence of metric and geometric properties of polyhedral surfaces. (2005) submitted.

[24] Federer, H.: Curvature measures. Transactions of the American Mathematical Society **93** (1959) 418–491

[25] Schoen, R., Yau, S.T.: Lectures on Differential Geometry. International Press, Cambridge, MA (1994)

[26] Gu, X., Wang, Y., Chan, T.F. Thompson, P. Yau, S-T.: Genus zero surface conformal mapping and its application to brain surface mapping. IEEE Trans. Med. Imaging. **23** (2004) 949–958

[27] Gu, X., Yau, S-T.: Global Conformal Parameterization. Symposium on Geometry Processing. (2003) 127–137

[28] Luo, W.: Error Estimates for Discrete Harmonic 1-forms Over Riemann Surfaces. Communications in Analysis and geometry. **14**,(2006)

[29] Jin, M., Luo, F., Gu, X.: Computing surface hyperbolic structure and real projective structure. In: ACM SPM. (2006) 105-116

[30] Chow, B., Luo, F.: Combinatorial Ricci flows on surfaces. Journal of Differential Geometry. **63** (2003) 97–129

[31] Alliez, P., Meyer, M., Desbrun, M.: Interactive geometry remeshing. ACM Trans. Graph. **21** (2002) 347–354

[32] He, Y., Wang, K., Wang, H., Gu, X., Qin, H.: Manifold T-spline. In: GMP. (2006) 409–422

[33] Gu, X., He, Y., Qin, H.: Manifold splines. Graphical Models. **68** (2006) 237–254

[34] He, Y., Gu, X., Qin, H.: Automatic shape control of triangular *B*-splines of arbitrary topology. Journal of Computer Science and Technology. **21** (2006) 232–237